Ronald M. Aarts

Tracking and Estimation of Frequency, Amplitude, and Form Factor of a Harmonic Time Series

Formulas for estimating and tracking the (time-dependent) frequency, form factor, and amplitude of harmonic time series are presented in this lecture note; in particular, sine-dominant signals, where the harmonics follow roughly the dominant first harmonic, such as photoplethysmography (PPG) and breathing signals. Special attention is paid to the convergence behavior of the algorithm for stationary signals and the dynamic behavior in case of a transition to another stationary state. The latter issue is considered to be important for assessing the tracking abilities for nonstationary signals. We will discuss special cases of sine-dominant signals that will converge to an approximate or the same value as for a single sinusoid. The presented formulas are recursive in nature and use only the instantaneous values of the signal, in a low-cost and low-complexity manner. In particular, there is no need to use square roots or trigonometric or matrix operations; therefore, these formulas are suitable for low-power ambulatory measurements and computationally demanding machine learning algorithms. Furthermore, there appears to be an interesting connection between the form factor and Geary's test of normality.

Digital Object Identifier 10.1109/MSP.2021.3090681
Date of current version: 27 August 2021

Relevance

In many engineering applications, such as those in astronomy, acoustics and communication, power-line frequency monitoring, power systems, spectroscopy, and audio engineering [1], one likes to know the frequency of a signal. Other applications are in (acoustic) velocity measurements of the Doppler shift, frequency-shift keying, sonar, estimating and interpreting the instantaneous frequency of a signal, and biomedical engineering. However, the focus here will be on PPG. This is a simple and low-cost optical technique that can be used to detect blood-volume changes in a microvascular bed of tissue [2], [3]. PPG is ubiquitous in clinical settings but also fast growing outside the clinic because it facilitates ambulatory monitoring. Athletes measure heart rates using a PPG sensor built into smart watches. Furthermore, PPG is used for sleep monitoring, atrial fibrillation detection [4], [5], epilepsy detection [6], and blood pressure measurement [7].

There is a vast amount of literature on frequency tracking, including a textbook [8]. While most published algorithms (see, e.g., [8]) are advanced and not very suitable for real-time signal processing, the algorithm proposed in this article strives for maximum efficiency, by avoiding division and trigonometric operations such as the fast Fourier transform—which also necessitates the use of buffers—and the like. This makes it suitable for low-power ambulatory measurements. Yet another application is that the efficient algorithm can be used in iterations of machine learning algorithms, like deep learning. Another difference is that the advanced methods are meant for tracking in bad signal-to-noise ratios (SNRs), making their range of applications different from what is envisaged here. We pay special attention to the convergence behavior of the algorithm for stationary signals and the dynamic behavior in case of a transition to another stationary state. The latter issue is considered important for assessing the tracking abilities for nonstationary signals.

Prerequisites

Basic background on calculus, algebra, and trigonometry, in addition to an overview on reference [9], will help readers, allowing for a better comprehension of this lecture note.

Problem statement

In an earlier article [9], a tracking algorithm was derived meant for single sinusoidal signals. In the following, an improvement is made in that the new algorithm can track harmonic time sequences with a more robust tracking behavior against amplitude changes and with an even slightly higher efficiency

in the required computational power. We shall show in our main result that a simple recursion can be used to get a good approximation of the normalized frequency of a signal.

The form factor f of a signal is defined as the ratio of the root-mean-square (RMS) value to the mean absolute value (MAV):

$$f = \frac{x_{\mathrm{RMS}}}{x_{\mathrm{MAV}}}. \tag{1}$$

The MAV is also known as the *average rectified value*. Today the form factor is not often used in physiological signal analysis, but it is hypothesized here that it may be useful in detecting physiological changes, e.g., in the morphology of a PPG signal. Furthermore, it can be used as a feature in machine learning algorithms. The emphasis of this article is on harmonic time series; however, the presented formula for the form factor tracker can be applied for general signals. We shall show that an efficient recursion of the form factor can be used. Furthermore, there appears to be an interesting connection between the form factor and Geary's test of normality.

Solution: Derivation of tracking formulas

Derivation of frequency tracking formulas

Considering that x is a harmonic time-series, where x_j is the input signal at time instance j, we start by examining (5), drawn from the paper in [9], i.e., Adelson's equation for rapid measurement of the frequency of a sine wave.

$$r = \frac{\sum_{j=1}^{n-1} x_j (x_{j-1} + x_{j+1})}{2\sum_{j=1}^{n-1} x_j^2}, \tag{2}$$

where the index k might be used to denote the time dependency of ω_0 as

$$r_k = \cos(\omega_{0,k} T_s). \tag{3}$$

Particularly, in such a case, r_k is the normalized frequency of a signal, ω_0 is its frequency, k the time index, and $f_s = 1/T_s$ the sampling frequency. To make this formula suitable for tracking purposes, (2) with $n = 2$ is modified to

$$r_{2,k} = \frac{x_{k-1}(x_{k-2} + x_k)}{2x_{k-1}^2}, \tag{4}$$

where the scalar 2 on the left-hand side is not an index. Instead, it is used just to emphasize the quadratic nature of the numerator and denominator of (4). In the present article, we modify (4) as

$$r_k = \frac{|x_{k-2} + x_k|}{2|x_{k-1}|}. \tag{5}$$

As will appear later, the new algorithm is more suitable for tracking harmonic time series. Furthermore, $0 \le r_k \le 1$; consequently, there should hold $0 < f_0 \le f_s/4$. Finally, a second modification is made by averaging using an exponential window. Now we define (with indices n for numerator and d for denominator)

$$r_k = \frac{S_{n,k}}{S_{d,k}}, \tag{6}$$

where

$$S_{n,k} = \sum_{l=0}^{\infty} c\, \mathrm{e}^{-\eta l} |x_{k-l} + x_{k-l-2}|, \tag{7}$$

$$S_{d,k} = \sum_{l=0}^{\infty} 2c\, \mathrm{e}^{-\eta l} |x_{k-l-1}|, \tag{8}$$

$$c = 1 - \mathrm{e}^{-\eta}, \tag{9}$$

and η is a small but positive number that should be adjusted to the particular circumstances for which tracking of the frequency is required. We note that

$$S_{n,k} = \mathrm{e}^{-\eta} S_{n,k-1} + c|x_k + x_{k-2}|, \tag{10}$$

and

$$S_{d,k} = \mathrm{e}^{-\eta} S_{d,k-1} + 2c|x_{k-1}|. \tag{11}$$

Hence, from the definition in (6),

$$r_k = \frac{S_{n,k-1} + c\, \mathrm{e}^{\eta} |x_k + x_{k-2}|}{S_{d,k-1} + 2c\, \mathrm{e}^{\eta} |x_{k-1}|}. \tag{12}$$

Since we consider small values of η, we have that $c = 1 - \mathrm{e}^{-\eta}$ is small as well. Expanding the right-hand side of (12) in powers of c and retaining only the constant and the linear term, we get, after some calculations,

$$r_k = r_{k-1} + \frac{c\, \mathrm{e}^{\eta}}{S_{d,k-1}} [|x_k + x_{k-2}| - 2r_{k-1}|x_{k-1}|] + O(c^2). \tag{13}$$

Then, deleting the $O(c^2)$ term, we finally obtain our main result, the recursion

$$\hat{r}_k = \hat{r}_{k-1} + \gamma [|x_k + x_{k-2}| - 2|x_{k-1}|\hat{r}_{k-1}], \tag{14}$$

where we identify

$$x_{\mathrm{MAV}} = \frac{S_{d,k}}{2} \tag{15}$$

as the mean absolute value of x_k, for a sufficiently large k, and

$$\gamma = \frac{c\, \mathrm{e}^{\eta}}{2x_{\mathrm{MAV}}}, \tag{16}$$

which is a constant for a stationary signal x_k. Comparing this γ in (16) to the one of (15) in [9], it appeared that the latter γ was proportional to x_{RMS}^{-2}, making the tracking behavior of the present algorithm more robust to changes in the amplitude than the one in [9].

We observe at this point that we have obtained the recursion in (14) by applying certain approximations [as in (15)] and neglecting higher order terms. Therefore, it is not immediately obvious that the actual r_k of (3) and the solution of $\hat{r}$ of the recursion in (14) have the same value, in particular for large k. However, in the section "Analysis of the Solution of the Basic Recursion," we shall show that $\hat{r}$ and r are closely related for the purposes of frequency estimation.

Derivation of the form factor tracking formulas

To make (1) suitable for tracking purposes, we follow the same concept as in the section "Derivation of Frequency Tracking Formulas" and write (1) as

$$\hat{f}_k = \frac{\sqrt{S_{\mathrm{R},k}}}{S_{\mathrm{A},k}}, \tag{17}$$

where

$$S_{\mathrm{R},k} = S_{\mathrm{R},k-1}(1 - \gamma_{\mathrm{f}}) + x_k^2 \gamma_{\mathrm{f}}, \tag{18}$$

$$S_{\mathrm{A},k} = S_{\mathrm{A},k-1}(1 - \gamma_{\mathrm{f}}) + |x_k| \gamma_{\mathrm{f}}, \tag{19}$$

are approximations of x_{RMS}^2 and x_{MAV}, respectively, and γ_{f} is a small constant

determining the speed of convergence. To make (17) faster and more suitable for computationally demanding machine learning algorithms, it can be approximated with a Newton–Raphson iteration as

$$\hat{f}_k \approx \frac{\hat{f}_{k-1}}{2} + \frac{S_{\mathrm{R},k}}{2\hat{f}_{k-1} S_{\mathrm{A},k}^2}, \tag{20}$$

where $\hat{f}_0 = 1$, which, at the expense of an add operation, a few multiplications, and a division, facilitates the tracking of the form factor. This is almost as efficient as the computation of the normalized frequency $\hat{r}_k$ by (14), where no division was required.

The relation between Geary's test and the form factor

Geary's test of normality [11] is defined as the ratio of the mean deviation to the standard deviation. If x is a random value from a normal distribution with zero mean and standard deviation σ, then the average absolute value of x is

$$\begin{aligned}\overline{|x|} = x_{\mathrm{MAV}} &= \frac{1}{\sigma\sqrt{2\pi}} \int_{-\infty}^{\infty} |x|\, e^{\frac{-x^2}{2\sigma^2}} dx \\ &= \sqrt{\frac{2}{\pi}}\,\sigma,\end{aligned} \tag{21}$$

and the average RMS value is

$$\begin{aligned}\sqrt{\overline{x^2}} &= x_{\mathrm{RMS}} \\ &= \sqrt{\frac{1}{\sigma\sqrt{2\pi}} \int_{-\infty}^{\infty} x^2 e^{\frac{-x^2}{2\sigma^2}} dx} = \sigma.\end{aligned} \tag{22}$$

Hence, Geary's ratio is equal to $\sqrt{2/\pi}$. In our notation [see (1)], Geary's ratio is equal to the inverse of the form factor, f^{-1}, and the form factor for Gaussian noise is equal to $\sqrt{\pi/2} \approx 1.25331$.

Analysis of the solution of the basic recursion

In this section, we consider the basic recursion in (14), and we analyze its solution $\hat{r}_k$, given an initial value $\hat{r}_0$ at $k = 0$, when $\gamma \downarrow 0$. We do this by reformulating the recursion in (14) so that it assumes the same form as the recursion used in [10]. It appears to be convenient to introduce the new variables

$$\beta_k = 2|\,x_{k-1}\,|, \tag{23}$$

and

$$\delta_k = |\,x_k + x_{k-2}\,|. \tag{24}$$

Thus, we shall consider the recursion in (14), which we rewrite as

$$\hat{r}_k = (1 - \gamma\beta_k)\hat{r}_{k-1} + \gamma\delta_k \tag{25}$$

for $k = 1, 2, \ldots$, with γ a small positive parameter.

In [10] it was shown, using Wiener's Tauberian theorem, how to obtain the limiting behavior of $\hat{r}_k$ as $k \to \infty$ when $\gamma > 0$ is small. This was done under an assumption (slightly stronger than required) that the mean values for the discrete-time case (denoted by M [.]),

$$\begin{aligned}b_0(\gamma) &= \mathrm{M}\Big[\frac{-1}{\gamma}\log(1 - \gamma\beta_k)\Big] \\ &= \lim_{K\to\infty} \frac{1}{K} \sum_{l=1}^{K} \frac{-1}{\gamma}\log(1 - \gamma\beta_l), \\ d_0 &= \mathrm{M}[\delta_k] = \lim_{K\to\infty} \frac{1}{K} \sum_{l=1}^{K} \delta_l,\end{aligned} \tag{26}$$

and for the corresponding continuous-time case,

$$\begin{aligned}b_0 &= \mathrm{M}[\beta(t)] = \lim_{T\to\infty} \frac{1}{T} \int_0^T \beta(t)\ \mathrm{d}t, \\ d_0 &= \mathrm{M}[\delta(t)] = \lim_{T\to\infty} \frac{1}{T} \int_0^T \delta(t)\ \mathrm{d}t,\end{aligned} \tag{27}$$

exist. Since $b_0(\gamma) \to b_0$ as $\gamma \downarrow 0$, it was shown in [10] that

$$\lim_{\gamma\downarrow 0}\Big[\lim_{k\to\infty} \hat{r}_k\Big] = \frac{\mathrm{M}[\delta_k]}{\mathrm{M}[\beta_k]} = \frac{d_0}{b_0} = \frac{\mathrm{M}[\delta(t)]}{\mathrm{M}[\beta(t)]}, \tag{28}$$

and, for any number $b < b_0(\gamma)$, that

$$\hat{r}_k = \frac{d_0}{b_0(\gamma T_s)} + O(e^{-\gamma b k}), \quad k \geq 0. \tag{29}$$

This shows that the time constant, i.e., the time $t = kT_s$ for the exponential term to drop to e^{-1} of its original value, for the tracking behavior is given by

$$\tau = \frac{T_s}{\gamma b_0(\gamma T_s)}. \tag{30}$$

We finally observe that $b_0(\gamma) \to b_0$ as $\gamma \downarrow 0$.

Likewise, for the derivation of (28), there holds for the form factor

$$\lim_{\gamma\downarrow 0}\Big[\lim_{k\to\infty} \hat{f}_k\Big] = f. \tag{31}$$

In the next section, we shall work this out for harmonic signals x.

Sinusoidal and harmonic input signals

In this section, we test the algorithms derived in the section "Derivation of Tracking Formulas" and analyzed in the preceding section with respect to the steady-state behavior, for sinusoidal input signals. Hence, we take

$$x_k = A_0 \sin(\omega_0 k T_s + \phi) \tag{32}$$

with arbitrary $A_0 > 0$ and ϕ.

Frequency tracker

Calculating β and δ with (23) and (24) and the corresponding b_0 and d_0 with (27) yields $b_0 = 4A_0/\pi$ and $d_0 = (4/\pi)$ $A_0 \cos(\omega_0 T_s)$. Now using (28), it is easy to obtain that

$$\lim_{\gamma\downarrow 0}\Big[\lim_{k\to\infty} \hat{r}_k\Big] = \cos\omega_0 T_s. \tag{33}$$

We compare this with (3) and note that this limit obviously does not depend on A_0 or ϕ. If (32) and $r_{k-1} = \cos\omega_0 T_s$ are substituted into (14), then we get $r_k = r_{k-1}$, independent of γ, indicating that r remains at a constant converged value. Using (30), it appears that the time constant of the tracking behavior is equal to

$$\tau = \frac{\pi T_s}{(4\gamma A_0)}. \tag{34}$$

For the case that the signal x consists of a sum of harmonic sinusoids,

$$x_k = A_0 \sum_{i=1,n} a_i \sin(i\omega_0 k T_s + \phi_i), \tag{35}$$

where $a_1 = 1, \phi_1 = 0$, and a_i and ϕ_i $(i \geq 2)$ are—loosely speaking—restricted such that the number of zero crossings of x_k is the same as for the case of a single sinusoid. See "The Nonsinusoidal-Phase Case" for more details. Hereafter, we will refer to those signals, like PPG and breathing signals, as sine-dominant signals, where the harmonics roughly

follow the dominant first harmonic. This is slightly more restrictive than necessary; however, it facilitates an easy calculation of the required integrals in (27), without being hampered by the absolute signs. Moreover, no knowledge of a_i is required because the condition is easily verified by observing x_k. For example, for $a_i = 1/i$ we obtain a PPG-like signal obeying this restriction (see "Nonnegative Sine Polynomials"). A wideband electrocardiographic signal, however, exhibits various undulations and therefore will not obey this restriction, unless it is band-limited in such a way that it has the same number of zero crossings as a single sinusoid of the same frequency. As an example, which will be discussed next in more detail, four sine-dominant (PPG-like) signals are shown in Figure 1.

The Nonsinusoidal-Phase Case

If $\phi_i \neq 0$, then the zero crossings of the harmonic signal given by (32) are not the same as those for a single sinusoid. Then we proceed as follows. Define the location of the first zero crossing close to $t = 0$ as $t_0 = \delta_0/\omega_0$ and the next one as $t_1 = \delta_1/\omega_0 + \pi/\omega_0$. Because we consider the signal as sine dominant, it is assumed that $|\delta_0, \delta_1| \ll 1$. Now, we calculate β and δ using (23) and (24) and the corresponding b_0 and d_0 with (27). The integrals now run from $t = t_0$ to $t = t_1$, and because we consider the signal as dc-free, it suffices to calculate the integrals only for this interval and get

$$\lim_{\gamma \downarrow 0}\Big[\lim_{k\to\infty} \hat{r}_k\Big] = \frac{d_0}{b_0} = \frac{\sum_{i=1}^{n} \frac{a_i}{i}\cos(i\omega_0 T_s)(\cos(i\delta_0 + \phi_i) + (-1)^{n-1}\cos(i\delta_1 + \phi_i))}{\sum_{i=1}^{n} \frac{a_i}{i}(\cos(i\delta_0 + \phi_i) + (-1)^{n-1}\cos(i\delta_1 + \phi_i))}. \quad \text{(S1)}$$

We can consider a few special cases.

- If $\delta_0 = \delta_1$ then all even harmonics vanish.
- If all $\phi_i = 0$ for $i > 1$, then $\delta_0 = \delta_1 = 0$. Then the right-hand side of (S1) reduces to (36). This holds for cases I, II, and IV in Figure 1.
- If $\delta_0 = \delta_1 = 0$, then the right-hand side of (S1) reduces to

$$\frac{\cos\omega_0 T_s + \sum_{i=3,5,\ldots}\left(\frac{a_i\cos(\phi_i)}{i}\right)\cos(i\omega_0 T_s)}{1 + \sum_{i=3,5,\ldots}\left(\frac{a_i\cos(\phi_i)}{i}\right)}. \quad \text{(S2)}$$

- If $\delta_0 = \delta_1 = 0$ and $\phi_i = \pm\pi/2$ for odd $i > 1$, or if $i\delta_0 + \phi_i = i\delta_1 + \phi_i = \pm\pi/2$ for odd $i > 1$, then the right-hand side of (S1) reduces to $\cos\omega_0 T_s$.
- The right-hand side of (36), (S1), and (S2) can be written as

$$\frac{\cos\omega_0 T_s + \Delta_n}{1 + \Delta_d}. \quad \text{(S3)}$$

For some cases like the preceding one, $\Delta_{n,d} = 0$. Otherwise, we can approximate (S3) by multiplying its numerator and denominator by $1 - \Delta_d$. Assuming $\Delta_{n,d} \ll 1$ and ignoring the higher order terms, we get

$$\cos\omega_0 T_s + \Delta_n - \Delta_d\cos\omega_0 T_s. \quad \text{(S4)}$$

If $\cos i\omega_0 T_s \approx 1$, then $\Delta_n \approx \Delta_d$ and (S1)–(S4) can be approximated as

$$\cos\omega_0 T_s. \quad \text{(S5)}$$

Nonnegative Sine Polynomials

The classic Fejér–Jackson–Gronwall inequality

$$\sum_{k=1}^{n} \frac{\sin(kx)}{k} > 0 \quad (n \geq 1; 0 < x < \pi) \quad \text{(S6)}$$

is one of the first inequalities for sine polynomials that appeared in the literature. The validity of (S6) was conjectured by Fejér in 1910, and later, many proofs, refinements, and generalizations followed, including Vietoris's last article, written at the age of 103. See [12] for a recent overview.

To let x_k be sine dominant, then for $n \geq 1$ and $\delta_0 < \omega_0 k T_s < \pi + \delta_1$,

$$x_k = A_0 \sum_{i=1}^{n} a_i \sin(i\omega_0 k T_s + \phi_i) > 0, \quad \text{(S7)}$$

and for $n \geq 1$ and $\pi + \delta_1 < \omega_0 k T_s < 2\pi + \delta_0$,

$$x_k = A_0 \sum_{i=1}^{n} a_i \sin(i\omega_0 k T_s + \phi_i) < 0, \quad \text{(S8)}$$

where $\delta_{0,1}$ are small numbers, say $|\delta_{0,1}| < 1$, $A_0 > 0$, $a_1 = 1$, and $\phi_1 = 0$. Because x_k is dc-free, its integral over time from δ_0 to $\pi + \delta_1$ is equal, but with opposite sign to that from the interval $\pi + \delta_1$ to $2\pi + \delta_0$. For cases I, II, and IV in Figure 1, $\delta_0 = \delta_1 = 0$; for case III, δ_0 and δ_1 are determined numerically as ≈ -0.146 and ≈ -0.157, respectively.

First, we calculate β and δ for the case that all harmonics are in sine phase (35) with all $\phi_i = 0$, using (23) and (24), and the corresponding b_0 and d_0, using (27). The integration is then straightforward, and we get

$$\lim_{\gamma \downarrow 0}\left[\lim_{k\to\infty} \hat{r}_k\right] = \frac{d_0}{b_0} = \frac{\cos\omega_0 T_s + \sum_{i=3,5,\ldots}\left(\frac{a_i}{i}\right)\cos(i\omega_0 T_s)}{1+\sum_{i=3,5,\ldots}\left(\frac{a_i}{i}\right)}. \quad (36)$$

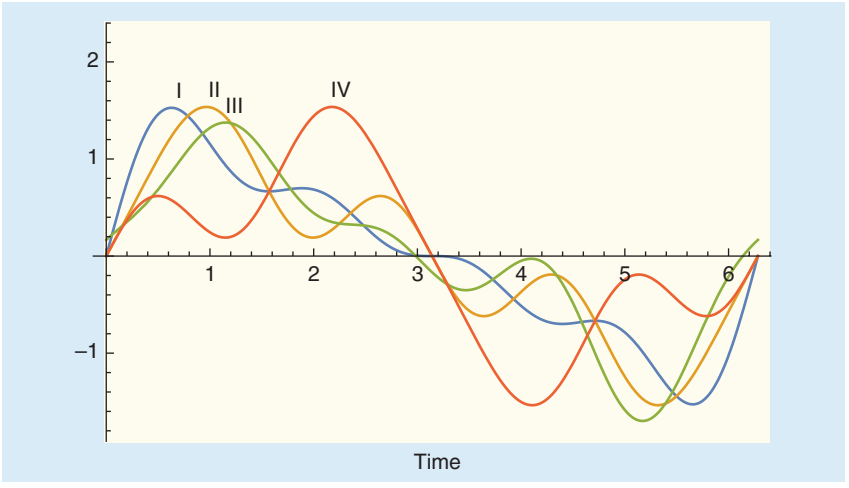

FIGURE 1. An example of four sine-dominant (PPG-like) signals using (35) versus time for one period ($\omega_0 T_s = 2\pi$). I (blue): $a_2 = 1/2, a_3 = 1/3, a_4 = 1/4$; II (orange): $a_2 = 1/2, a_3 = 1/3, a_4 = -1/4$; III (green): $a_2 = 1/2, a_3 = 1/6, a_4 = -1/4$; IV (red): $a_2 = -1/2, a_3 = 1/3, a_4 = 1/4$. All $\phi_i = 0$, but for case III, $\phi_3 = \pi/2$.

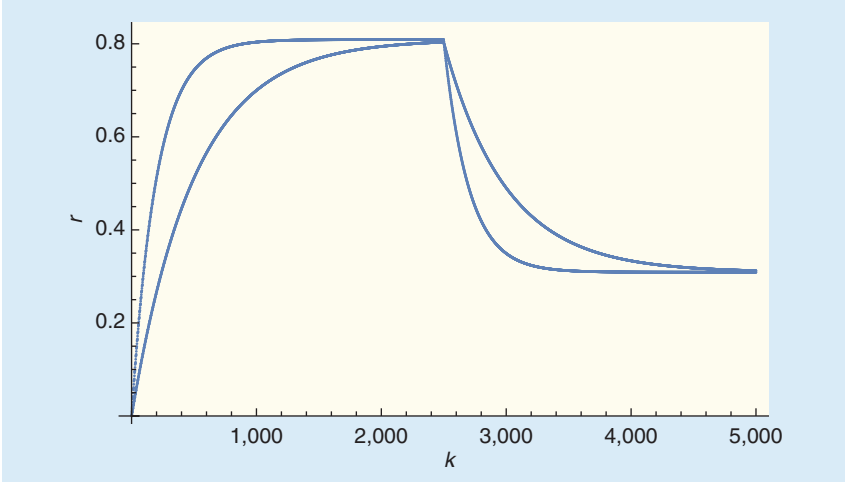

FIGURE 2. An example of r versus $k = t/T_s$, using (14) with amplitude $A_0 = 1, \hat{r}_0 = 0$, making a step from $\omega_0 T_s = \pi/5$ ($r = 0.81$) to $\omega_0 T_s = 2\pi/5$ ($r = 0.31$). The values for the parameter γ are 1/500 and 1/250, respectively; the latter value is causing the steeper edges in r.

Table 1. The influence of uniformly (U) and Gaussian-distributed (G) wideband noise on the average error $\bar{\epsilon}$ of $\hat{r}_k - \cos(\omega_0 T_s)$ and its variance σ^2_{ϵ}.

SNR [dB]	$\bar{\epsilon}_U$	$\sigma^2_{\epsilon,U}$	$\bar{\epsilon}_G$	$\sigma^2_{\epsilon,G}$
20	–2.84 E-3	1.76 E-6	–1.82 E-3	2.08 E-6
10	–7.83 E-3	1.88 E-5	–5.37 E-3	2.27 E-5
0	–4.44 E-2	9.71 E-5	–4.25 E-2	1.06 E-4
–10	–1.25 E-1	6.29 E-4	–9.33 E-2	5.60 E-4
–20	–1.14 E-1	2.35 E-3	–1.07 E-1	1.96 E-3

Here we see that A_0 and the terms with even i vanish and the odd terms come with a factor a_i/i. If the latter are known, then (36) can be solved iteratively to obtain $\cos(\omega_0 T_s)$. The general phase case ($\phi_i \neq 0$) is discussed in "The Nonsinusoidal-Phase Case." There it was found that, under certain assumptions, we can approximate $\hat{r}$ as $\hat{r} \approx \cos\omega_0 T_s$, which is independent of a_i, ϕ_i and is the same result as that for a single sinusoidal input signal (33).

Example

To demonstrate the tracking behavior of (14), in Figure 2 the step response is plotted for a sinusoidal input signal, making a change in frequency, for two values of γ. It appears that the time constants correspond well with the values predicted by (34). The values of γ used in Figure 2 are just for illustration purposes; they may be much larger. To obtain stability, we need $|1 - \beta_k \gamma| < 1$. Practical values for sinusoidal input signals are $0 < A_0\gamma < 0.5$.

Noise influence

To study the influence of noise, a simulation was performed by adding wideband uniformly and Gaussian-distributed noise, respectively, to a single sinusoid of fixed frequency ($\omega_0 T_s = \pi/5$). Then, with $\gamma = 1/500$, the average error $\bar{\epsilon}$ of $\hat{r}_k - \cos(\omega_0 T_s)$ and its variance σ^2 of 100,000 iterations of (14) was computed, for various levels of SNRs. See Table 1 for the results.

It appears from Table 1 that $\hat{r}$ computed by (14) is rather insensitive to both types of wideband noise. Through SNRs as low as 0 dB, the average error in $\hat{r}$ is on the order of a few percent. In practice, the signal will be band-limited to the frequency band of interest, and hence the error will decrease for the same wideband noise power.

Amplitude tracker

To compute A_0 of the input signal x_k (for the case $\delta_0 = \delta_1 = 0$; see "The Nonsinusoidal-Phase Case"), (11), (27), (35), and (S2) are combined, resulting in

$$\hat{A}_{0,k} = \frac{\pi S_{d,k}}{4\left[1 + \sum_{i=3,5,\ldots} \left(\frac{a_i \cos(\phi_i)}{i}\right)\right]}, \quad (37)$$

where $\hat{A}_{0,k}$ is the estimate for A_0.

Form factor tracking

We calculate the form factor f for the case that all harmonics are in sine phase (35) (all $\phi_i = 0$) by integration of x_k^2 and $|x_k|$, for the numerator and denominator of (1), respectively, as

$$f = \frac{\pi}{2\sqrt{2}} \frac{\sqrt{\sum_{i=1,2,3,\ldots} a_i^2}}{\sum_{i=1,3,5,\ldots} \left(\frac{a_i}{i}\right)}. \quad (38)$$

Here, we see that f in (38) is independent of A_0, and its denominator is dependent only on odd a_i. For a simple single sinusoid, (38) reduces to the well-known form $\pi/2\sqrt{2} \approx 1.1107$. For the examples shown in Figure 1, we get both by applying either (38) as well as (18)–(20), the same value $f \approx 1.19273$, where it has been verified that applying (17) or (20) does not show a practical difference. In the section "The Relation Between Geary's Test and the Form Factor," it was shown that the form factor for Gaussian noise is equal to $\sqrt{\pi/2} \approx 1.25331$, and it has also been verified that (20) converges to this value as well.

What we have learned

This article has presented formulas for tracking the frequency, form factor, and amplitude of a harmonic signal in real time. The proposed method (14) aims at lowering the computational complexity compared to other methods. It has been shown that this method contains only a few arithmetic operations and is insensitive to the initial value and noise. The behavior of the algorithm has been shown to provide satisfactory accuracy for harmonic signals as inputs.

Acknowledgments

This paper was written during the COVID-19 lockdown. Nevertheless, the author is grateful to Dr. Massimo Mischi, who reviewed an earlier draft of the article, and to Dr. A.J.E.M. Janssen for discussing the topic and earlier drafts of this article. Moreover, his help was not limited to this article but has extended over the period of the last 20 years.

Author

Ronald M. Aarts (r.m.aarts@tue.nl) received his B.Sc. degree in electrical engineering in 1977 and his Ph.D. degree in physics from Delft University in 1995. He joined Philips Research Labs in 1977 and initially investigated servos and signal processing for CD players. Then he extended his interests in engineering to medicine and biology and in particular to sensors, signal processing, and systems for ambulatory and unobtrusive monitoring, sleep, cardiology, perinatology, and epilepsy detection. Since 2006, he has been a professor with the Signal Processing Systems group at Eindhoven University of Technology, Eindhoven, 5600 MB, The Netherlands. He has been president of Aarts Consultancy since 1990. He has published more than 400 papers and more than 100 granted U.S. patents. He is a Fellow of IEEE.

References

[1] E. Larsen and R. M. Aarts, *Audio Bandwidth extension. Application of Psychoacoustics, Signal Processing and Loudspeaker Design.* Hoboken, NJ: Wiley, Sept. 2004.

[2] J. Allen, "Photoplethysmography and its application in clinical physiological measurement," *Physiol. Meas.*, vol. 28, no. 3, pp. R1–R39, 2007. doi: 10.1088/0967-3334/28/3/R01.

[3] R. M. Aarts, "Overview of Photoplethysmography (PPG) related papers produced by TU/e-SPS' chair on Ambulatory Monitoring." Aug. 20, 2020. [Online]. Available: https://www.sps.tue.nl/rmaarts/RMA_papers/aar20mi17.pdf

[4] A. G. Bonomi et al., "Atrial fibrillation detection using photo-plethysmography and acceleration data at the wrist," in *Proc. Comput. Cardiol. Scientific Conf. (CinC 2016)*, Vancouver, Canada, Sept. 11–14, 2016, pp. 277–280.

[5] L. M. Eerikäinen et al., "Detecting atrial fibrillation and atrial flutter in daily life using photoplethysmography data," *IEEE J. Biomed. Health Inform.*, vol. 24, no. 6, pp. 1610–1618, June 2020. doi: 10.1109/JBHI.2019.2950574.

[6] J. van Andel et al., "Using photoplethysmography in heart rate monitoring of patients with epilepsy," *Epilepsy Behav.*, vol. 45, pp. 142–145, Apr. 2015. doi: 10.1016/j.yebeh.2015.02.018.

[7] G. Zhang et al., "Hybrid optical unobtrusive blood pressure measurements," *Sensors*, vol. 17, no. 7, p. 1541, 2017. doi: 10.3390/s17071541.

[8] G. Quinn and E. J. Hannan, *The Estimation and Tracking of Frequencies*. Cambridge, U.K.: Cambridge Univ. Press, 2001.

[9] R. M. Aarts, "Low-complexity tracking and estimation of frequency and amplitude of sinusoids," *Digital Signal Process.*, vol. 14, no. 4, pp. 372–378, July 2004. doi: 10.1016/j.dsp.2004.03.001.

[10] R. M. Aarts, R. Irwan, and A. J. E. M. Janssen, "Efficient tracking of the cross-correlation coefficient," *IEEE Trans. Speech Audio Process.*, vol. 10, no. 6, pp. 391–402, Sept. 2002. doi: 10.1109/TSA.2002.803447.

[11] R. C. Geary, "The ratio of the mean deviation to the standard deviation as a test of normality," *Biometrika*, vol. 27, nos. 3–4, pp. 310–332, Oct. 1935. doi: 10.2307/2332693.

[12] H. Alzer and M. K. Kwong, "Classes of nonnegative sine polynomials," in *Trigonometric Sums and Their Application*, A. Raigorodskii and M. Rassias, Eds. Cham: Springer-Verlag, 2020, pp. 71–84.

SP